

See discussions, stats, and author profiles for this publication at: <https://www.researchgate.net/publication/269416628>

Bicomponent H-Bonded Porous Molecular Networks at the Liquid–Solid Interface: What Is the Influence of Preorganization in Solution?

ARTICLE in LANGMUIR · DECEMBER 2014

Impact Factor: 4.46 · DOI: 10.1021/la5027398 · Source: PubMed

READS

62

3 AUTHORS:



Tibor Kudernac

University of Twente

45 PUBLICATIONS 2,205 CITATIONS

[SEE PROFILE](#)



Amal kumar Mandal

University of Twente

34 PUBLICATIONS 494 CITATIONS

[SEE PROFILE](#)



Jurriaan Huskens

University of Twente

365 PUBLICATIONS 8,291 CITATIONS

[SEE PROFILE](#)

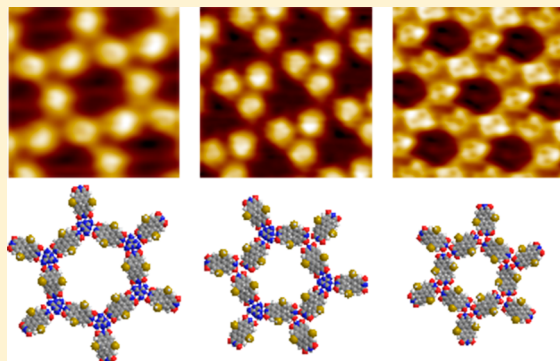
Bicomponent H-Bonded Porous Molecular Networks at the Liquid–Solid Interface: What Is the Influence of Preorganization in Solution?

Tibor Kudernac,* Amal Kumar Mandal, and Jurriaan Huskens

Molecular Nanofabrication Group, MESA+ Institute for Nanotechnology, University of Twente, P.O. Box 217, Enschede 7500AE, The Netherlands

Supporting Information

ABSTRACT: Tailoring the architecture of porous two-dimensional networks formed by molecules is essential for developing functional materials with low dimensionality. Here we present bicomponent porous networks with tunable pore-sizes that were formed by self-assembly of hydrogen-bonding molecules at the liquid/graphite interface. Scanning tunneling microscopy investigations demonstrate the formation and coexistence of three polymorphs. It is found that the occurrence of these polymorphs depends critically on the surface coverage. Further on, atomic force microscopy measurements, spectroscopic studies, and dynamic light scattering investigations show the propensity of one of the two molecular components to form aggregates beyond the monolayer. We discuss how these preorganized aggregates in solution may affect the self-assembly at the interface.



INTRODUCTION

The self-assembly of molecules on surfaces is paving the way toward the ultimate nanostructuring of two-dimensional optoelectronic materials directly interfaced to the macroscale.¹ Porous molecular networks on surfaces, in particular, attract a lot of attention, as their pores can immobilize molecules with a variety of properties and functions in a regular and preprogrammed manner.² Furthermore, their porous character allows for positioning of dynamic functional groups that require space for their operation.³ Pores of molecular networks were also used to confine the self-assembly of thiols on a nanometre scale.⁴ Ultimately, it is believed that, provided with the right functional groups, these molecular pores could catalyze molecular transformation with a truly nanoscale control and high selectivity.^{5,6}

Paving the way toward these achievements requires the development of molecular nanoporous networks that are robust, modular, and predictable. Bicomponent molecular networks stabilized by multiple hydrogen-bonds are most likely to meet these criteria, as they are constructed and stabilized by highly directional and relatively strong supramolecular interactions.⁷ Moreover, one or both of the components can be readily substituted, thus forming a network with a new structure and properties. Bicomponent H-bonded nanoporous networks have been successfully constructed on solid surfaces under ultrahigh vacuum (UHV) conditions.^{7,8} The typical approach to achieve the open porous structure involves deposition of the two components in the appropriate ratio and in a submonolayer coverage regime. This ensures that the self-assembled structures, with an additional aid of annealing when necessary, will be able to expand into open networks.

Although this process is conceptually relatively straightforward, the experimental execution and finding the optimal conditions is a costly and time-consuming process, and the resulting structures remain stable only under UHV conditions.

Forming molecular networks on surfaces at ambient conditions and more particularly at liquid–solid interfaces remains a challenge as phase separation and polymorphism are likely to occur at these conditions.⁹ The first porous networks prepared by dip coating of gold samples in solution were composed of melamine and perylene tetracarboxylic diimide (PTCDI) as building blocks.⁴ Arguably, the self-assembled structure that was formed was far from equilibrium, which impairs the reproducibility of this approach and its wide adaptation to other H-bonded systems including those with identical binding motifs and shorter naphthalene tetracarboxylic diimide molecules.¹⁰ Self-assembled monolayers of a one to one mixture of melamine and cyanuric acid were successfully formed on highly oriented pyrolytic graphite (HOPG) under thermodynamic control.¹¹ However, these structures featured only pores with moderate sizes of approximately 0.6 nm in diameter, which limits their use in encapsulating molecular guests.¹² Porous structures with larger pores were formed under thermodynamic control by self-assembly of melamine as a three-fold connector unit and bis-uracil functionalized rod-like molecules.^{9,13} Relatively small ordered crystalline domains of porous structures were found on surfaces together with disordered structures and glassy structures with irregular

Received: July 11, 2014

Revised: December 8, 2014



ACS Publications

© XXXX American Chemical Society

A

DOI: 10.1021/la5027398
Langmuir XXXX, XXX, XXX–XXX

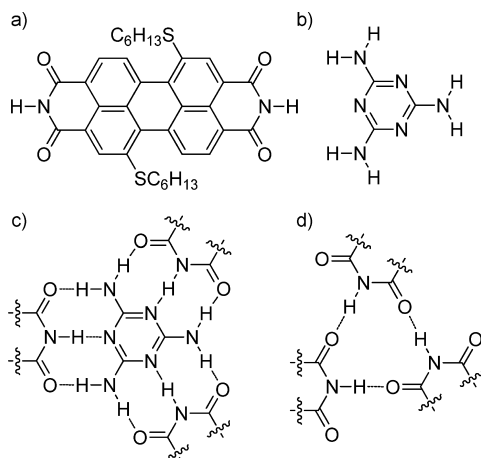
pores. Creating bicomponent H-bonded nanoporous networks at liquid–solid interfaces and under thermodynamic control thus remains a challenge.

Here, we build on the use of PTCDI and melamine as building blocks and show that nanoporous networks are formed under thermodynamic control at the interface between HOPG and 1,2,4-trichlorobenzene (TCB). Moreover, we show that the geometry of these monolayers can be tuned by controlling molecular preorganization in solution.

■ EXPERIMENTAL SECTION

PTCDI-SC6 (Scheme 1a) was synthesized according to the previously developed strategy.¹⁴ All STM experiments were carried out at 20–24

Scheme 1. (a) Molecular Structure of Perylene Tetracarboxylic Diimide Derivative PTCDI-SC6; (b) Molecular Structure of Melamine; (c) Complementary Hydrogen-Bonding Motif Formed between One Molecule of Melamine with Three PTCDI-SC6 Molecules; and (d) Self-Complementary Hydrogen-Bonding Motif That Links Three Molecules of PTCDI-SC6¹⁴



°C. Experiments were performed using a PicoSPM microscope (Agilent). Tips were mechanically cut from PtIr wire (80:20 alloy, diameter 0.25 mm). Prior to imaging, solutions of PTCDI-SC6 and melamine in 1,2,4-trichlorobenzene were prepared and mixed to form appropriate concentrations (PTCDI-SC6: 10, 19, 38, 76, 152 to 300 μM, melamine: 13, 25, 50, 100, 200). For each experiment, a drop of the appropriate solution was applied onto a freshly cleaved surface of HOPG (grade ZYB, Advanced Ceramics Inc., Cleveland, OH). The STM investigations were then performed at the liquid–solid interface within 2 h of the initial drop-casting of the solution (unless stated otherwise). This ensures that the concentration changes do not significantly affect the self-assembly process. For each concentration, the experiments were also repeated up to three times, depending on the success with achieving submolecular resolution of the monolayer. The data that are presented correspond to the highest resolution images at the concentration of interest. The HOPG lattice was recorded by lowering the bias after obtaining images of the 2D structure. Images were corrected for drift effects using the HOPG lattice as a calibration grid (Scanning Probe Image Processor (SPIP) 5.1.8 software (Image Metrology ApS)). STM investigations at the liquid–solid interface were also attempted with the use of other high boiling point solvents, including tetradecane, phenyloctane, and octanol. The solubility of the PTCDI-SC6 and/or melamine was, however, below the micromolar range, and no ordered structures were observed. Additionally, octanoic acid was used as a solvent that solubilized the molecules in the micromolar range. The only structure that was observed upon codeposition of PTCDI-SC6 and melamine

was the previously reported coassembly of melamine with octanoic acid.¹⁵ UV-vis spectra were obtained using a UV-spectrometer PerkinElmer Lambda 850. Steady-state emission spectra at room temperature were obtained using a fluorescence spectrometer (PerkinElmer). Dynamic light scattering (DLS) measurements were performed on a Zetasizer NanoZS (Malvern Instrument Ltd, Malvern, United Kingdom) with a laser wavelength of $\lambda = 633$ nm and a scattering angle of 173°.

■ RESULTS AND DISCUSSION

Preliminary experiments with PTCDI did not yield any regular molecular patterns at the liquid–HOPG interface either on its own or in combination with melamine, most likely because of its low solubility in usual organic solvents (not shown). Consequently, we functionalized PTCDI with two thioalkoxy side groups forming PTCDI-SC6 (Scheme 1a),¹⁴ in order to increase its solubility in common organic solvents. Scheme 1c shows the three-fold symmetry of the diaminopyridine–diimide complementary H-bonding motif between melamine and three PTCDI-SC6 molecules that yields extended porous networks. In the absence of melamine, PTCDI-SC6 can form a porous network via self-complementary H-bonding also as was demonstrated under UHV conditions (Scheme 1d).¹⁴

When a solution of PTCDI-SC6 and melamine (3:2) in TCB ($[PTCDI-SC6]_{TCB} = 38 \mu\text{M}$ and $[melamine]_{TCB} = 25 \mu\text{M}$) was drop-casted on the freshly cleaved surface of HOPG, the molecules formed porous honeycomb structures spontaneously (Figure 1a). Figure 1b shows a high resolution scanning tunneling microscopy (STM) image obtained by cross-correlation analysis of the same area.¹⁶ The unit cell parameters of these structures are $a = 3.32 \pm 0.2 \text{ nm}$, $b = 3.31 \pm 0.2 \text{ nm}$, and $\alpha = 61 \pm 2^\circ$, with an average area occupied by the unit cell $A = 9.4 \pm 0.6 \text{ nm}^2$. An average distance of two facing edges from their center is about 3.3 nm. This corresponds well with the molecular model of the expected honeycomb structure for a 3:2 self-assembly of PTCDI-SC6 and melamine, in which the number of H-bonds is maximized (Scheme 1c). Consequently, we will refer to this structure as the P3M2 structure. The STM contrast is dominated by the bright signal attributed to the aromatic core of PTCDI-SC6. Melamine molecules are not visible under these tunneling conditions, which is also in accordance with previous studies.^{4,17}

Surprisingly, two other types of porous structures were observed at the same concentration of PTCDI-SC6 and melamine (Figure 1d–i). The pores in these structures are distinctively smaller compared to the pores in the P3M2 structure. One of these two structures (Figure 1d) is characterized by unit cell parameters $a = 2.96 \pm 0.3 \text{ nm}$, $b = 2.93 \pm 0.2 \text{ nm}$, and $\alpha = 60 \pm 4^\circ$ with an average area occupied by the unit cell $A = 7.6 \pm 0.7 \text{ nm}^2$. The high resolution STM image obtained by cross-correlation analysis of the same area shows an equilateral hexagonal pore (Figure 1e). One pore is constituted by six bright protrusions that are ascribed to PTCDI-SC6 molecules. The center of each of these bright protrusions is separated from its neighbors by approximately 1.4 and 1.7 nm, respectively. Given the length of PTCDI-SC6 (~1.25 nm based on a minimized molecular structure) the separation of 1.4 nm does not allow for a molecule of melamine to be included: three neighboring PTCDI-SC6 molecules form a trimer stabilized by three H-bonds (Scheme 1d). However, the distance of 1.7 nm is identical to the distances measured for the P3M2 structures, which suggests that melamine is incorporated in this case, and nine H-bonds are formed

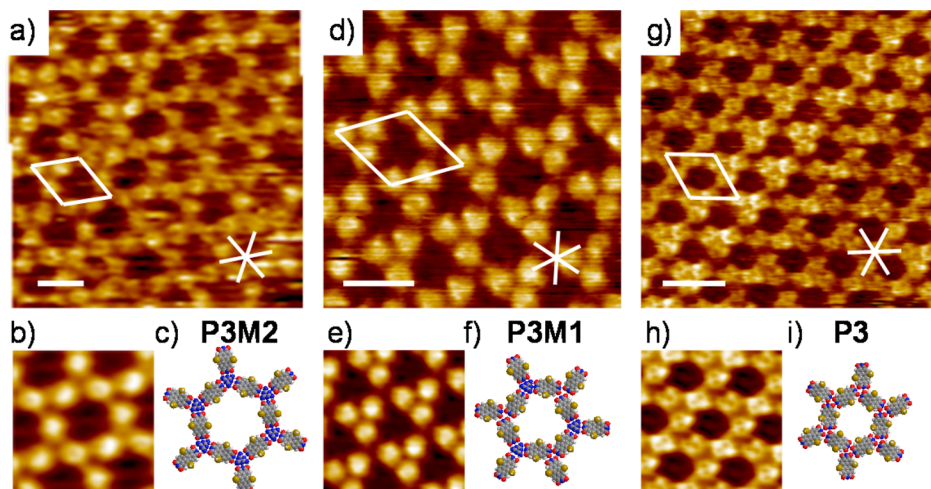


Figure 1. STM images and molecular models of porous monolayers formed by self-assembly of PTCDI-SC6 and melamine at the TCB/HOPG interface ($38 \mu\text{M}$ and $25 \mu\text{M}$ by referring to the individual components in the same solution). All presented images originate from the same experiment. The white stars indicate the orientation of the main axis of the underlying HOPG surface and the white scale bars correspond to 3 nm . (a) P3M2 porous network with a unit cell (indicated by the white parallelogram) formed by three PTCDI-SC6 and two melamine molecules, $V_T = 445 \text{ mV}$, $i_T = 21 \text{ pA}$, $19 \times 19 \text{ nm}^2$. (b) High-resolution image ($V_T = 445 \text{ mV}$, $i_T = 21 \text{ pA}$, $6 \times 6 \text{ nm}^2$) obtained by cross-correlation.¹⁶ (c) Molecular model showing the P3M2 molecular packing. (d) P3M1 porous network with a unit cell (indicated by the white parallelogram) formed by three PTCDI-SC6 and one melamine molecules, $V_T = 505 \text{ mV}$, $i_T = 21 \text{ pA}$, $12 \times 12 \text{ nm}^2$. (e) High-resolution image ($V_T = 505 \text{ mV}$, $i_T = 21 \text{ pA}$, $6 \times 6 \text{ nm}^2$) obtained by cross-correlation.¹⁶ (f) Molecular model showing the corresponding molecular packing. (g) P3 porous network with a unit cell (indicated by the white parallelogram) formed by three PTCDI-SC6 molecules, $V_T = 505 \text{ mV}$, $i_T = 21 \text{ pA}$, $15 \times 15 \text{ nm}^2$. (h) High-resolution image ($V_T = 505 \text{ mV}$, $i_T = 21 \text{ pA}$, $6 \times 6 \text{ nm}^2$) obtained by cross-correlation.¹⁶ (i) Molecular model showing the corresponding P3 molecular packing.

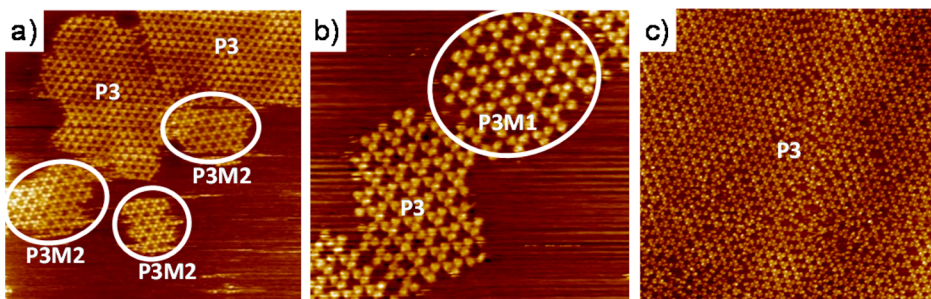


Figure 2. (a,b) STM images of hydrogen-bonded structures formed from the TCB solution of PTCDI-SC6 and melamine at submonolayer coverage ($38 \mu\text{M}$ and $25 \mu\text{M}$), (a) $V_T = 445 \text{ mV}$, $i_T = 21 \text{ pA}$, $84 \times 84 \text{ nm}^2$ and (b) $V_T = 505 \text{ mV}$, $i_T = 21 \text{ pA}$, $40 \times 40 \text{ nm}^2$. White circles highlight the area of the surface where the P3M2 structure (a) and P3M1 structure (b) is formed. (c) STM image of hydrogen-bonded P3 structures formed from the TCB solution of PTCDI-SC6 and melamine at full-monolayer coverage ($[\text{PTCDI-SC6}]_{\text{TCB}} = 152 \mu\text{M}$ and $[\text{melamine}]_{\text{TCB}} = 100 \mu\text{M}$), $V_T = 445 \text{ mV}$, $i_T = 22 \text{ pA}$, $67 \times 67 \text{ nm}^2$.

between three PTCDI-SC6 molecules and melamine (Scheme 1c). The corresponding structural model is shown (Figure 1f). Because one unit cell is composed of three molecules of PTCDI-SC6 and one molecule of melamine, this structure will be referred to as the P3M1 structure.

The unit cell parameters of the smallest porous structure (Figure 1g) are $a = 2.68 \pm 0.1 \text{ nm}$, $b = 2.70 \pm 0.2 \text{ nm}$, and $\alpha = 62 \pm 3^\circ$, with an average area occupied by the unit cell $A = 6.4 \pm 0.5 \text{ nm}^2$. The STM contrasts obtained by cross-correlation analysis of the same area are more structured, and the orientation of individual PTCDI-SC6 molecules is visible (Figure 1h). A pair of bright contrast dots featured in each molecule originates from two sulfur atoms that are known to yield intense STM contrasts.¹⁸ The distances between the PTCDI-SC6 molecules do not allow for adsorption of additional melamine molecules. Identical porous structures are also formed when a solution of pure PTCDI-SC6 in TCB is drop-casted on HOPG (Supporting Information (SI) Figure S1). This porous structure is stabilized by self-complementary

H-bonding (Scheme 1d). Each pore is constituted by six PTCDI-SC6 molecules (Figure 1i), which corresponds to a unit cell composed of three molecules. This structure will be referred to as the P3 structure. The average size of the pores is 2.7 nm , and the center of each molecule is equally separated from the center of the four neighboring molecules by 1.4 nm . Apparent distances between the edges of the bright protrusions vary across the images due to in-commensuration of the structure with respect to HOPG. This also results in the appearance of moiré waves (SI Figure S2).

The coexistence of the aforementioned porous structures is observed only at the submonolayer regime (Figure 2a,b). The P3M2 and P3M1 structures exist as isolated islands or at the edges of the ordered areas (Figure 2a,b). Together, P3M2 and P3M1 form less than 30% of the ordered structure. The remaining areas of the surface occupied by molecules were covered by the P3 structure. Other types of ordered structures including self-assembled domains of melamine molecules were not observed. A similar self-assembly was observed upon

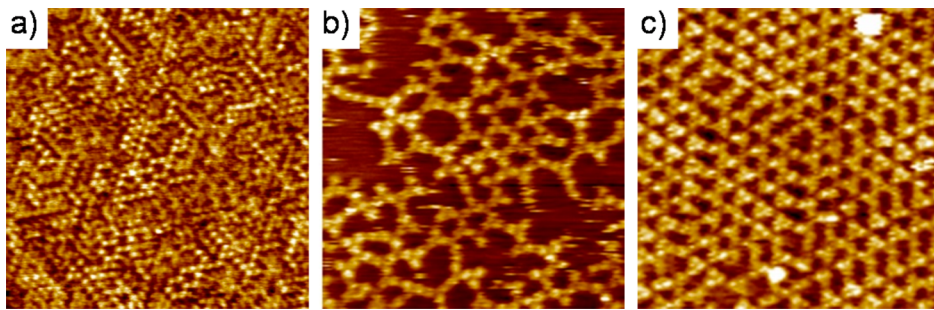


Figure 3. STM images of the HOPG surface area of $33 \times 33 \text{ nm}^2$ following the stepwise deposition of melamine and PTCDI-SC6. (a) Preformed melamine monolayer, $V_T = 610 \text{ mV}$, $i_T = 21 \text{ pA}$. (b) STM image taken 5 min after an addition of PTCDI-SC6 solution, $V_T = 480 \text{ mV}$, $i_T = 26 \text{ pA}$. (c) STM image recorded 25 min after the addition of PTCDI-SC6 solution, $V_T = 480 \text{ mV}$, $i_T = 26 \text{ pA}$.

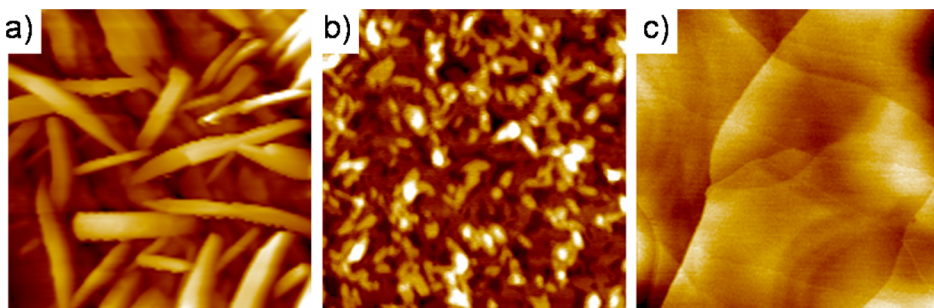


Figure 4. (a) AFM image acquired at the tapping mode of the aggregates formed on HOPG from a mixed solution of PTCDI-SC6 and melamine with $[\text{PTCDI-SC6}]_{\text{TCB}} = 152 \mu\text{M}$ and $[\text{melamine}]_{\text{TCB}} = 100 \mu\text{M}$, respectively, $1.6 \times 1.6 \mu\text{m}^2$. (b) AFM image of PTCDI-SC6 aggregates on HOPG formed by drop-casting a $[\text{PTCDI-SC6}]_{\text{TCB}} = 152 \mu\text{M}$ solution, $0.82 \times 0.82 \mu\text{m}^2$. (c) AFM height image of a HOPG surface where a droplet of $100 \mu\text{M}$ melamine solution in TCB was drop-casted, $2.20 \times 2.20 \mu\text{m}^2$. HOPG steps are clearly visible, while no aggregates can be detected.

decreasing the concentration of PTCDI-SC6 down to $19 \mu\text{M}$. Below this concentration, self-assembly does not occur at the interface. Changes in the ratio of the components from 3:2 to 1:10 of PTCDI-SC6 to melamine within these concentrations yielded the same results. At a concentration of $152 \mu\text{M}$ of PTCDI-SC6 and $100 \mu\text{M}$ of melamine, the surface reaches full coverage. At this and higher concentrations, only domains of P3 structure were observed (Figure 2c). The larger pores observed in the image are defects between individual domains. Within the measured range of the changing ratio of PTCDI-SC6 and melamine (3:2 to 1:10 ratio of PTCDI-SC6 to melamine at concentrations of PTCDI-SC6 higher than $38 \mu\text{M}$) P3M2 and P3M1 structures or melamine self-assembly have not been observed. Within the time scale of the measurements (5 min to 2 h) no structural evolution or transition between the P3M2, P3M1, and P3 structures has been observed at the given concentration besides dissolutions of small domains, probably due to their decreased stability against scanning conditions.

Drop-casting of a solution of pure melamine in TCB ($[\text{melamine}]_{\text{TCB}} = 100 \mu\text{M}$) onto HOPG resulted in the formation of self-assembled monolayer (Figure 3a). Although some local order could be found, the overall monolayer is disordered. Disordered domains of melamine were observed at submonolayer coverage also (SI Figure S3). Addition of PTCDI-SC6 (a $[\text{PTCDI}]_{\text{TCB}} = 152 \mu\text{M}$ droplet of similar volume) immediately led to the formation of irregular porous structures containing mainly PTCDI-SC6 molecules (Figure 3b). Melamine molecules were either not visible or they were not adsorbed. Within 25 min, the irregular structures were replaced, and the surface was fully covered by PTCDI-SC6 molecules (Figure 3c). This robustness of the system with

respect to the starting (initial) conditions and the sequential deposition suggests that the self-assembly process is thermodynamically driven and that P3 structures are approaching the equilibrium state. To further support this claim, we annealed the PTCDI-SC6 structure formed by a 3:2 PTCDI-SC6/melamine mixture ($38 \mu\text{M}$ and $25 \mu\text{M}$), for 2 h up to 80°C . The annealing treatment did not result in any alteration of the packing geometry (SI Figure S4).

In order to understand the thermodynamic stability of P3, we compared it to the P3M2 structure that is intuitively more stable. We discuss here a qualitative estimate of the relative stabilization energies of these two structures on HOPG, while neglecting the presence of the solution. For P3M2, the stabilization energy by hydrogen bonding is 4.4 eV per unit cell, as the sum of $12 \text{ O}\cdots\text{H}-\text{N}$ and six $\text{N}\cdots\text{H}-\text{N}$ bonds.¹⁹ The adsorption energy of two melamine and three PTCDI-SC6 molecules on HOPG is 0.36 eV ($2 \times 0.18 \text{ eV}$)¹³ and 4.11 eV ($3 \times 1.37 \text{ eV}$), respectively.²⁰ The combined stabilization energy per unit cell is 8.91 eV and per nm^2 is $0.95 \text{ eV}/\text{nm}^2$. The P3 structure is stabilized by six $\text{O}\cdots\text{H}-\text{N}$ bonds per unit cell. The stabilization energy of this hydrogen bonding motive is not known and considered here as $1/3$ of the P3M2 structure (1.47 eV). This is an overestimation of the stabilization energy that neglects the cooperativity effect of the tridentate hydrogen bonding in the P3M2 structure. The additional energy gain from the adsorption of three PTCDI-SC6 molecules (4.11 eV) gives the stabilization energy per unit cell of 5.58 eV and per nm^2 of $0.87 \text{ eV}/\text{nm}^2$. Despite the conservative estimate that the hydrogen stabilization of P3M2 is only 3 times larger than that for the P3 structure, the stabilization energy of P3M2 per nm^2 is considerably larger. Other intermolecular interactions, such as van der Waals and dipole–dipole interactions, are not

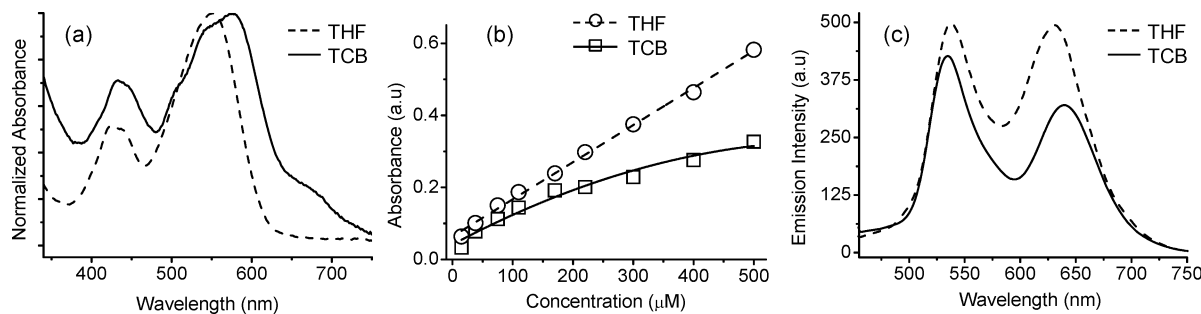


Figure 5. (a) Normalized UV-vis absorption spectra of PTCDI-SC6 ($15 \mu\text{M}$) recorded in 1,2,4-trichlorobenzene (TCB) and tetrahydrofuran (THF) at room temperature. (b) Absorbance of PTCDI-SC6 at the absorption maxima ($\lambda_{\text{max},\text{TCB}} = 575 \text{ nm}$ and $\lambda_{\text{max},\text{THF}} = 545 \text{ nm}$) with varying concentration (15 – $500 \mu\text{M}$). (c) Fluorescence spectra of PTCDI-SC6 ($1 \mu\text{M}$) recorded in TCB and THF at room temperature upon excitation at ($\lambda_{\text{exc.}} = 435 \text{ nm}$).

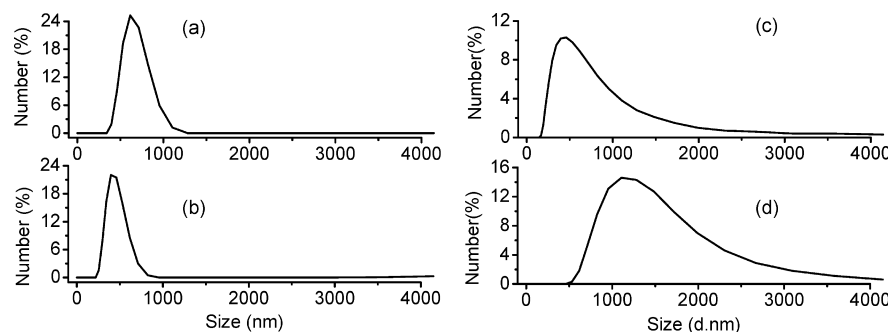


Figure 6. DLS graph measured in 1,2,4-trichlorobenzene (TCB) at room temperature for (a) (3:2) mixture of PTCDI-SC6 ($38 \mu\text{M}$) and melamine ($25 \mu\text{M}$); (b) PTCDI-SC6 ($38 \mu\text{M}$); (c) (3:2) mixture of PTCDI-SC6 ($400 \mu\text{M}$) and melamine ($270 \mu\text{M}$); and (d) PTCDI-SC6 ($400 \mu\text{M}$).

expected to play an important role here, while repulsive intermolecular interactions due to induced interfacial dipolar moments will further favor the more expanded **P3M2** structure.²¹ The contribution of the alkyl chains to the overall stabilization of the structures is not expected to differ considerably as the sizes of the pores allow for their complete adsorption on the surfaces, while the hexagonal symmetry of the pores prevents effective lateral interactions. On the basis of these considerations, we conclude that it is unlikely that the preferred formation of the **P3** structure can be explained solely based on molecule–molecule and molecule–substrate interactions.

Going beyond the first layer, the self-assembly of the 3:2 mixture of PTCDI-SC6 and melamine in TCB, on HOPG, was investigated by means of atomic force microscopy (AFM). The solution of PTCDI-SC6 and melamine ([PTCDI]_{TCB} = $152 \mu\text{M}$ and [melamine]_{TCB} = $100 \mu\text{M}$), was drop-casted onto HOPG. The excess solution was removed with a stream of nitrogen gas. This procedure ensures that the amount of molecules on the dry surface is not dramatically increased by drying. The AFM height image shows that larger molecular aggregates are formed under these conditions (Figure 4a). PTCDI-SC6 (drop-casted from a [PTCDI-SC6]_{TCB} = $152 \mu\text{M}$ solution and dried) forms aggregates, even in the absence of melamine (Fig. 4b). The aggregates are in this case smaller probably due to a higher rate of aggregation that is not influenced by the competing interactions. However, a solution of pure melamine in TCB ([melamine]_{TCB} = $100 \mu\text{M}$) does not yield any visible aggregates under similar conditions (Figure 4c).

In order to explore whether PTCDI-SC6 and melamine self-assemble in TCB and/or in tetrahydrofuran (THF), prior to

their deposition on a surface, we performed spectroscopic measurements. The UV-vis spectrum of $15 \mu\text{M}$ solution of PTCDI-SC6 in TCB shows two distinct bands, which are characteristics for two different electronic transitions, the S_0 – S_1 with absorption maximum at 575 nm and the S_0 – S_2 with absorption maximum at 435 nm (Figure 5a).^{22,23} The S_0 – S_1 transition shows two vibronic bands at 575 nm and a shoulder at 545 nm (Figure 5a). Another band shoulder is observed around 675 nm (Figure 5a).

Upon increasing the concentration of PTCDI-SC6, the vibronic structure becomes even more prominent and the intensity of the transition also increases (SI Figure S5a). In contrast, in such a polar solvent as THF,²⁴ the absorption band for S_0 – S_1 transition is blue-shifted (545 nm) and appears with no vibronic structure (Figure 5a) even at very high concentration (SI Figure S5b). The gradual changes of absorbance at λ_{max} are shown in Figure 5b for various concentrations of PTCDI-SC6. The nonlinear increase of absorbance in TCB suggests that PTCDI-SC6 is present in an aggregated form. In polar THF, however, PTCDI-SC6 is present as individually dissolved molecules, as demonstrated by the linear increase of the absorbance. These observations are in good agreement with previous literature reports.^{25,26} Adding 0.6, 1.5, 2.5, 3.5, and 5 equiv of melamine to a $20 \mu\text{M}$ solution of PTCDI-SC6 in TCB does not considerably change the absorption spectra (SI Figure S6). The moderate overall increase of the absorbance and the absence of shifts in the absorption maxima upon increase of the melamine concentration suggest that melamine is likely not included in the aggregates, however, they could influence the size of the aggregates by modifying the polarity of the solution.²⁷

The fluorescence spectra of PTCDI-SC6 in TCB and THF support this argument further. In both solvents, two emission maxima were observed when the molecule was excited at the S_0 - S_2 transition (Figure 5c). However, an appreciable decrease in emission intensity and a red shift in the emission maximum were observed in TCB. This again suggests that in TCB, PTCDI-SC6 molecules exist in an aggregated form, where efficient electron transfer is responsible for the observed luminescence quenching and the red shift in the emission maximum.^{28,29}

We have measured the particle size distribution of the aggregates by dynamic light scattering (DLS) also, in order to investigate the self-assembly of PTCDI-SC6 and melamine in solution. A broad particle size distribution was observed for the aggregates formed both by PTCDI-SC6 and by the (3:2) mixture of PTCDI-SC6 and melamine at two different concentrations (Figure 6). For a PTCDI-SC6 concentration of 38 μM , the aggregates have an average diameter of 396 nm (Figure 6b). In the presence of melamine, the particle size distribution as well as the average diameter of the aggregates increased to 615 nm (Figure 6a). However, the diameter measured by DLS should be taken with caution as DLS is not well-suited for investigating nonspherical objects. At higher concentration of PTCDI-SC6 (400 μM) the particle size distribution as well as the average diameter of the aggregates increased compared to its low concentration (Figure 6c,d). In this case, the presence of melamine in the solution (270 μM) leads to a decrease in size of the aggregates (Figure 6c). Importantly, a solution of melamine alone at the corresponding concentrations ($[\text{melamine}]_{\text{TCB}} = 270 \mu\text{M}$ and $[\text{melamine}]_{\text{TCB}} = 25 \mu\text{M}$) never did yield any measurable DLS signal.

While one intuitively expects that aggregation in solution should heavily influence self-assembly at the liquid–solid interface, this preorganization is usually neglected, likely because proving and/or understanding such an effect is not a trivial task. The formation of aggregates in solution can in principle influence the self-assembly of molecules on surfaces through two mechanisms; (a) preorganizing molecules in solution, that subsequently adsorb on a surface as larger aggregates and (b) modifying the effective concentration of components in multicomponent systems. In the present system, PTCDI-SC6 molecules show a higher propensity to form both stable monolayer structures and larger aggregates both in solution and on the surface of HOPG upon drying. A decrease of the effective concentration of PTCDI-SC6 is therefore not likely to be the reason for the observed self-assembly at the liquid–solid interface. Alternatively, we suggest that the PTCDI-SC6 aggregates that were observed in solution might imprint their structure on the surface. Elucidating the mechanism for imprinting a supramolecular structure from the solution onto the surface is not trivial. The structure formed at the interface is highly dynamic and easy to exchange with the structure present in solution, and many molecular aggregates in the proximity of the surface are likely to interact with it. However, we can propose that when a favorable facet of the aggregate comes into contact with the surface, the first molecular layer of the aggregate physisorbs on the surface in order to decrease the surface energy. Release of the aggregate from the surface is more likely to happen by peeling off a few layers of the aggregate rather than by desorption of all molecules, constituting it as the latter would lead to an increase of the surface energy. As the surface might slightly stretch/compress the first molecular layer to compensate for the

incommensurability, the peeling between the first and second layer would be the most probable scenario. Further on, such an imprinting mechanism of monolayer formation would be kinetically and entropically favored compared to the process where the molecules need to be first dissolved from the aggregate and subsequently reassembled into the surface structure.

It remains unclear whether the solution phase aggregates have the same symmetry or whether the molecules that come into contact with the surface rapidly rearrange. Common closed-packed self-assembled structures based on PTCDI molecules on a surface³⁰ were not observed for PTCDI-SC6 probably due to the presence of peripheral side groups. The same preference for the formation of porous structures can in principle take place during aggregation in solution. These protruding peripheral side groups do not allow the molecules to orient themselves side-by-side in a densely packed aggregate of parallel chains stabilized by hydrogen bonding. The most densely packed 3D structures that would be both stabilized by hydrogen bonding and would provide sufficient space for the side chains can be realized by layering the observed P3 structure to form 3D aggregates. We were not able to obtain conclusive solution diffraction data or to grow a crystal of PTCDI-SC6 that would help us to unequivocally elucidate the structure of the PTCDI-SC6 aggregates. Further studies will aim at establishing the exact relationship between the solution phase aggregates and the self-assembled structures at the interface.

CONCLUSIONS

We have described the fabrication of bicomponent nanoporous molecular networks composed of a perylene tetracarboxylic diimide derivative PTCDI-SC6 and melamine on graphite. At submonolayer coverage we evidenced the coexistence of structures in which the pores have different sizes and shapes. The unit cell of these structures is composed of the two molecular building blocks in varying proportions. At full-monolayer coverage, however, melamine is not adsorbed on the surface of graphite, and the molecular pores are entirely composed of PTCDI-SC6. The preference for the formation of a monocomponent monolayer at full coverage is attributed to the preorganization of the perylene derivative in solution. Our findings suggest that molecular processes occurring in solution cannot be neglected when investigating self-assembly at the liquid–solid interface.

ASSOCIATED CONTENT

S Supporting Information

Experimental procedures, synthesis, and characterization, and additional STM images. This material is available free of charge via the Internet at <http://pubs.acs.org>.

AUTHOR INFORMATION

Corresponding Author

*E-mail: t.kudernac@utwente.nl.

Author Contributions

The manuscript was written through the contributions of all the authors. All authors have given approval to the final version of the manuscript.

Notes

The authors declare no competing financial interest.

ACKNOWLEDGMENTS

This research was supported by The Netherlands Organization for Scientific Research (NWO-CW) through a VENI grant (T.K.).

REFERENCES

- (1) Barth, J. V.; Constantini, G.; Kern, K. Engineering Atomic and Molecular Nanostructures at Surfaces. *Nature* **2005**, *437*, 671–679.
- (2) Bonifazi, D.; Mohnani, S.; Llanes-Pallas, A. Supramolecular Chemistry at Interfaces: Molecular Recognition on Nanopatterned Porous Surfaces. *Chem.—Eur. J.* **2009**, *15*, 7004–7025.
- (3) Tahara, K.; Inukai, K.; Adisoejoso, J.; Yamaga, H.; Balandina, T.; Blunt, M. O.; De Feyter, S.; Tobe, Y. Tailoring Surface-Confined Nanopores with Photoresponsive Groups. *Angew. Chem., Int. Ed.* **2013**, *52*, 8373–8376.
- (4) Madueno, R.; Räisänen, M. T.; Silien, C.; Buck, M. Functionalizing Hydrogen-Bonded Surface Networks with Self-Assembled Monolayers. *Nature* **2008**, *454*, 618–621.
- (5) Piot, L.; Bonifazi, D.; Samori, P. Organic Reactivity in Confined Spaces under Scanning Tunneling Microscopy Control: Tailoring the Nanoscale World. *Adv. Funct. Mater.* **2007**, *17*, 3689–3693.
- (6) Zhang, X.; Zeng, Q.; Wang, C. Molecular Templates and Nano-Reactors: Two-Dimensional Hydrogen Bonded Supramolecular Networks on Solid/Liquid Interfaces. *RSC Adv.* **2013**, *3*, 11351–11366.
- (7) Theobald, J. A.; Oxtoby, N. S.; Phillips, M. A.; Champness, N. R.; Beton, P. H. Controlling Molecular Deposition and Layer Structure with Supramolecular Surface Assemblies. *Nature* **2003**, *424*, 1029–1031.
- (8) Xu, W.; Wang, J.-G.; Jacobsen, M. F.; Mura, M.; Yu, M.; Kelly, R. E. A.; Meng, Q.-Q.; Lægsgaard, E.; Stensgaard, I.; Linderoth, T. R.; Kjems, J.; Kantorovich, L. N.; Gothelf, K. V.; Besenbacher, F. Supramolecular Porous Network Formed by Molecular Recognition between Chemically Modified Nucleobases Guanine and Cytosine. *Angew. Chem., Int. Ed.* **2010**, *49*, 9373–9377.
- (9) Palma, C.-A.; Bjork, J.; Bonini, M.; Dyer, M. S.; Llanes-Pallas, A.; Bonifazi, D.; Persson, M.; Samori, P. Tailoring Bicomponent Supramolecular Nanoporous Networks: Phase Segregation, Polymorphism, and Glasses at the Solid–Liquid Interface. *J. Am. Chem. Soc.* **2009**, *131*, 13062–13071.
- (10) Teyssandier, J.; Battaglini, N.; Seydou, M.; Anquetin, G.; Diawara, B.; Sun, X.; Maurel, F.; Lang, P. Elaboration of Hydrogen-Bonded 2D Supramolecular Assemblies on Au(111) From Solutions: Toward Naphthalene Tetracarboxylic Diimide–Melamine Nanoporous Networks. *J. Phys. Chem. C* **2013**, *117*, 8737–8745.
- (11) Zhang, X.; Chen, T.; Chen, Q.; Wang, L.; Wan, L.-J. Self-Assembly and Aggregation of Melamine and Melamine–Uric/Cyanuric Acid Investigated by STM and AFM on Solid Surfaces. *Phys. Chem. Chem. Phys.* **2009**, *11*, 7708–7712.
- (12) Kudernac, T.; Lei, S.; Elemans, J. A. A. W.; De Feyter, S. Two-Dimensional Supramolecular Self-Assembly: Nanoporous Networks on Surfaces. *Chem. Soc. Rev.* **2009**, *38*, 402–421.
- (13) Palma, C.-A.; Bonini, M.; Llanes-Pallas, A.; Breiner, T.; Prato, M.; Bonifazi, D.; Samori, P. Pre-Programmed Bicomponent Porous Networks at the Solid–Liquid Interface: The Low Concentration Regime. *Chem. Commun.* **2008**, 5289–5291.
- (14) Perdigao, L. A.; Saywell, A.; Fontes, G. N.; Staniec, P. A.; Goretzki, G.; Phillips, A. G.; Champness, N. R.; Beton, P. H. Functionalized Supramolecular Nanoporous Arrays for Surface Templating. *Chem.—Eur. J.* **2008**, *14*, 7600–7607.
- (15) Walch, H.; Maier, A.-K.; Heckl, W. M.; Lackinger, M. Isotopological Supramolecular Networks from Melamine and Fatty Acids. *J. Phys. Chem. C* **2009**, *113*, 1014–1019.
- (16) The image was obtained by cross-correlation of a zoomed-in area over a larger area of the same self-assembly domain using SPIP software (Image Metrology).
- (17) Silly, F.; Shaw, A. Q.; Castell, M. R.; Briggs, G. A. D. A Chiral Pinwheel Supramolecular Network Driven by the Assembly of PTCDI and Melamine. *Chem. Commun.* **2008**, 1907–1909.
- (18) Cyr, D. M.; Venkataraman, B.; Black, A.; Whitesides, G. M.; Flynn, G. W. Functional Group Identification in Scanning Tunneling Microscopy of Molecular Adsorbates. *J. Phys. Chem.* **1996**, *100*, 13747–13759.
- (19) Sassi, M.; Oison, V.; Debierre, J.-M. First Principle Study of a Bimolecular Thin Film on Ag(1 1 1) Surface. *Surf. Sci.* **2008**, *602*, 2856–2862.
- (20) The adsorption energy of PTCDI-SC6 is estimated as adsorption energy of a polycyclic aromatic hydrocarbon of 24 carbon atoms with the incremental energy per carbon atom of 0.057 eV according to the following: Thrower, J. D.; Friis, E. E.; Skov, A. L.; Nilsson, L.; Andersen, M.; Ferrighi, L.; Jørgensen, B.; Baouche, S.; Balog, R.; Hammer, B.; Hornekær, L. Interaction between Coronene and Graphite from Temperature-Programmed Desorption and DFT-vdW Calculations: Importance of Entropic Effects and Insights into Graphite Interlayer Binding. *J. Phys. Chem. C* **2013**, *117*, 13520–13529. The four carbons of the carboxylic groups are included in this consideration which consequently overestimates the adsorption energy gain of the perylene (C20) part while the short aliphatic side chains are not considered.
- (21) Kudernac, T.; Sändig, N.; Fernandez Landaluce, T.; van Wees, B. J.; Rudolf, P.; Katsonis, N.; Zerbetto, F.; Feringa, B. L. Intermolecular Repulsion through Interfacial Attraction: Toward Engineering of Polymorphs. *J. Am. Chem. Soc.* **2009**, *131*, 15655–15659.
- (22) Gvishi, R.; Reisfeld, R.; Burshtein, Z. Spectroscopy and laser action of the “red perylimide dye” in various solvents. *Chem. Phys. Lett.* **1993**, *213*, 338–344.
- (23) Langhals, H. Cyclic carboxylic imide structures as structure elements of high stability. Novel Developments in perylene dye chemistry. *Heterocycles* **1995**, *40*, 477–500.
- (24) Sinks, L. E.; Rybtchinski, B.; Iimura, M.; Jones, B. A.; Goshe, A. J.; Zuo, X.; Tiede, D. M.; Li, X.; Wasielewski, M. R. Self-Assembly of Photofunctional Cylindrical Nanostructures Based on Perylene-3,4:9,10-bis(dicarboximide). *Chem. Mater.* **2005**, *17*, 6295–6303.
- (25) Würthner, F. Perylene bisimide dyes as versatile building blocks for functional supramolecular architectures. *Chem. Commun.* **2004**, 1564–1579.
- (26) van der Boom, T.; Hayes, R. T.; Zhao, Y.; Bushard, P. J.; Weiss, E. A.; Wasielewski, M. R. Charge Transport in Photofunctional Nanoparticles Self-Assembled from Zinc 5,10,15,20-Tetrakis-(perylene-3,4-dieneimide)porphyrin Building Blocks. *J. Am. Chem. Soc.* **2002**, *124*, 9582–9590.
- (27) Würthner, F.; Thalacker, C.; Sautter, A.; Schärtl, W.; Ibach, W.; Hollricher, O. Hierarchical Self-Organization of Perylene Bisimide–Melamine Assemblies to Fluorescent Mesoscopic Superstructures. *Chem.—Eur. J.* **2000**, *6*, 3871–3886.
- (28) Thalacker, C.; Würthner, F. Chiral Perylene Bisimide–Melamine Assemblies: Hydrogen Bond-Directed Growth of Helically Stacked Dyes with Chiroptical Properties. *Adv. Funct. Mater.* **2002**, *12*, 209–218.
- (29) Würthner, F.; Thalacker, C.; Diele, S.; Tschiesske, C. Fluorescent J-type Aggregates and Thermotropic Columnar Mesophases of Perylene Bisimide Dyes. *Chem.—Eur. J.* **2001**, *7*, 2245–2253.
- (30) Mura, M.; Silly, F.; Briggs, G. A. D.; Castell, M. R.; Kantorovich, L. N. H-Bonding Supramolecular Assemblies of PTCDI Molecules on the Au(111) Surface. *J. Phys. Chem. C* **2009**, *113*, 21840–21848.